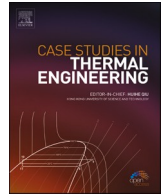




ELSEVIER

Contents lists available at [ScienceDirect](https://www.sciencedirect.com)

# Case Studies in Thermal Engineering

journal homepage: <http://www.elsevier.com/locate/csited>

## The comparative of the performance for predicted thermal models during microwave ablation process using a slot antenna

Wutipong Preechaphonkul, Phadungsak Rattanadecho<sup>\*</sup>

Center of Excellence in Electromagnetic Energy Utilization in Engineering (CEEE), Department of Mechanical Engineering, Faculty of Engineering, Thammasat University (Rangsit Campus), Pathumthani 12120, Thailand

### ARTICLE INFO

#### Keywords:

Microwave ablation  
Thermal ablation  
Comparative thermal model  
Porous media  
Bioheat  
Local thermal equilibrium (LTE)  
Liver cancer  
Numerical simulation

### ABSTRACT

Microwave (MW) ablation is a new technology for focused cancer treatment. This treatment applies the microwave power to tumor by using the MW antenna. The modeling for heat transport in the biological tissue was applied in the therapeutics application for preventing injury and analyzing the effectiveness of the treatment process. There were many heating models proposed for predicted heat transfer in the liver model. However, there were few studies comparative of the heating models in the liver cancer model. This study presented the systematically the comparative performance of the thermal model during the MW ablation process with MW power of 10 W and frequency of 2.45 GHz. The comparative thermal models implemented in this work were the bioheat model, the porous media model with constant velocity, and the Darcy-Brinkman porous model on the heat transfer in liver cancer model during MW ablation process. The mathematical models were considered to couple with electromagnetic wave propagation, heat transfer, and blood flow analysis. The Darcy-Brinkman porous model has a comparative advantage higher than the porous model with constant velocity. The Darcy-Brinkman porous model was effective in various situations of predictions as compared to other models, since the role of conduction and the role of convection were combined. The value of investigated provided an indication of limitations that must be considered in administering microwave ablation therapy.

### 1. Introduction

Microwave (MW) ablation is a new technology for focused cancer treatment. This treatment is an alternative treatment for liver cancer [1–3], which one of the cancers that have a low survival rate [4]. The MW ablation has applied the MW power to the target tissue (tumor) by MW antenna. The MW is absorbed and converted to the heat generation in the tumor. The tissue temperature rises to 52 °C for a heating time of 1 min, or the instantaneous tissue temperature exceeds 54 °C, the cell will be killed immediately [5–10]. The goal of this treat tissue by the MW heating and without damaging it to the surrounding tissue. Furthermore, MW ablation has many advantages and powerful treatment techniques compared with conventional treatment for localized liver cancer treatment. However, MW ablation has dangerous when used incorrect conditions during treatment, such as the heat spread over the boundaries of the tumor area. When the heat spread over the boundaries of the tumor, the temperature of healthy tissue is rising. The increase of the healthy tissue temperature is resulting in the protein denaturation process, which is dangerous on the healthy tissue. Therefore, the studies of correct conditions are necessary.

<sup>\*</sup> Corresponding author.

E-mail address: [ratphadu@engr.tu.ac.th](mailto:ratphadu@engr.tu.ac.th) (P. Rattanadecho).

<https://doi.org/10.1016/j.csited.2021.100908>

Received 26 April 2020; Received in revised form 23 February 2021; Accepted 25 February 2021

Available online 2 March 2021

2214-157X/© 2021 The Author(s). Published by Elsevier Ltd. This is an open access article under the CC BY-NC-ND license

(<http://creativecommons.org/licenses/by-nc-nd/4.0/>).

MW ablation is a popular treatment technique for primary and metastatic liver tumors [11–13], and has advantages over the other thermal ablation (such as radiofrequency ablation (RFA)) [14,15,16]). It could not apply to human liver beings due to be unethical. Many researchers have been experimenting with animals [10,17–21]). However, these experimental studies had limitations compared to experimenting with a nearly realistic human liver. The numerical simulation could be applied to study the treatment. It has been the advantage of needing only a short period, the low economic cost, humanity, and could be set up with conditions near to those of a real human liver. Most simulation studies of liver cancer treatment with thermal therapy used the Pennes bioheat model, introduced by Pennes [22].

The Pennes bioheat model has been widely applied in many studies about heat transfer in biological tissue, in particular, this has been applied in the thermal ablation models [23–25]. Although the Pennes bioheat model is widespread and has been applied in several studies, this model requires many assumptions and may limit their application [26]. Therefore, researchers proposed the new model, the modified bioheat model, or the couple bioheat with other models for reduced the many assumptions and highly accurate in the specific situations.

Wulff and Klinger proposed the new bioheat equation, pointing out the shortcomings of the Pennes bioheat model, because of not considering the moving blood through the biological tissue convect heat in any direction [27,28]. In 2007, Yang et al. developed a modified bioheat model for prediction temperature profiles during MW ablation in a high temperature state [29]. After that, Keangin et al. developed the numerical model of liver cancer treatment with MW ablation, which included thermal deformation analysis during the treatment process [2]. In 2016, Wu et al. proposed the model of MW ablation in liver tissue with the multi-frequency [30].

Although the bioheat model could be modified to improve accuracy and efficiency, the bioheat models have some limitations. This model cannot handle several physical effects, in particular, the directional of blood flow and convective heat transfer mechanism. Some researchers proposed the porous media model applied in the biological tissue for improved model accuracy and efficiency. The realistic, the biological tissue includes the cell, blood vessel, and interstitial space, which can be defined as the solid phase and fluid phase in the biological domain [31]. Therefore, the biological tissue could assume a porous structure [32,33]. Thus, the porous media theory can be applied in biological tissue [34]. In 2009, Mahjoob and Vafai proposed the hyperthermia treatment in the two biological models, based on the local thermal non-equilibrium (LTNE) model in porous media theory [31]. The advantages of utilizing a porous media model in biological tissue has few assumptions as compared to different established bioheat transfer models [31].

In 2013, the liver cancer with MW ablation treatment model based on the porous media approach was proposed by Rattanadecho & Keangin [34]. This work was the first study of heat transfer and blood flow in the two-layered porous liver during MW ablation process using single and double slot antenna. This study was considered the fluid with constant velocity but considered the fluid with fluid flow equations in the porous tissue domain. Keangin et al. presented the mathematical model of biological materials based on porous theory. This model imposed the electromagnetic field on biological materials such as the liver, brain, bone, and skin, etc. The results showed the effect of electromagnetic power and frequency on the temperature of solid phase and blood phase in biological materials [35]. After that, Keangin and Rattanadecho developed the porous liver cancer model during MW ablation treatment. The mathematical model based on LTNE approach and the equations of the model considered couple with electromagnetic wave propagation and heat transfer analysis. The simulation results showed the effect of the model approach, porosity, and MW power during MW ablation treatment [26].

Although the performing comparative of the predicted thermal models during the MW ablation process, there are a few studies. In particular, the systematical studies of the performing comparative heat modeling implemented in the biological tissue. Therefore, the porous model was applied in the biological tissue coupled with the blood flow model with the heat transfer model, which is necessary and exciting. The comparative of the thermal models during the MW ablation process on the heat transfer affects the accuracy and effectiveness of the liver cancer model. Furthermore, the systematic study of the different heating models in the early stage of heating time to the long stage of heating time has not appeared. Therefore, the fundamental of the different heating implemented could be selected as the suitable heat models for the right condition and situation.

This study proposed the performing comparative of the predicted heating models implemented of the liver cancer model with MW ablation with MW power of 10 W and frequency of 2.45 GHz. The heating models implemented were the bioheat model, the porous model with constant velocity, and the Darcy-Brinkman porous model. The porous models (the porous model with constant velocity and the Darcy-Brinkman porous model) were based on the local thermal equilibrium (LTE) approach. The mathematics of all models considered coupled with the electromagnetic wave propagation and heat transfer in the liver tissue. In the specific Darcy-Brinkman porous model deemed to be fully combined with the electromagnetic wave propagation, heat transfer, and flow analysis in the liver cancer model. The effect of the bioheat model, the porous model with constant velocity, and the Darcy-Brinkman porous model on the temperature distribution was systematically comparison. For accuracy, the numerical model was validated with experimental results by Yang et al. [29]. In finally, this study presented suitable models for prediction temperature profiles during MW ablation treatment for various conditions. The fundamental understanding of models could be a guideline for effective treatment.

## 2. Modeling and formulation

The anatomic structure of the model consists of the liver tissue domain and the MW antenna domain. The liver tissue domain (tumor and healthy tissue) as porous media materials consist of solid and fluid phases (blood phase), in which domains considered with electromagnetic wave propagation, heat transfer, blood flow analysis (Brinkman model extended Darcy). The MW antenna domain is less affected by heat transfer, therefore considered with electromagnetic wave propagation only. This study developed the numerical of liver cancer model with MW ablation based on the LTE porous model. Furthermore, this study investigated the performing comparative of the heating models implemented of the liver cancer treatment with MW ablation on the heat transfer.

**Table 1**  
Dimensions and dielectric properties of single slot MCA [2]].

Material	Dimensions (mm)	Dielectric properties		
		Relative permittivity, $\epsilon_r$	Electric conductivity, $\sigma_{el}$ (S/m)	Relative permeability, $\mu_r$
Inner conductor	0.135 (radial)	–	–	–
Dielectric	0.47 (radial)	2.03	0	1
Outer conductor	0.595 (radial)	–	–	–
Catheter	0.895 (radial)	2.1	0	1
Slot	1.00 (wide)	1	0	1

2.1. Problem description

MW ablation is a type of thermal ablation. This technique is using the MW frequency induced external heat in a specific area. The MW frequency is transmitted by using a MW antenna, in which the MW coaxial antenna (MCA) is used extensively [34]. This study was developed the numerical model of liver cancer treatment with MW ablation by using a single-slot MCA transmitting the MW power into a specific area (tumor domain). The single-slot MCA has a diameter of 1.79 mm, the antenna is required as small as a possible for minimally invasive [26]. A wide of the ring-shaped slot of 1 mm is cut off the outer conductor, and the length of 5.5 mm from the short-circuited tip, that for avoiding the electric field becomes stronger near the slot (Saito et al., 2000). The MW antenna operated at the power of 10 W and frequency of 2.45 GHz, which is used for MW ablation treatment. The dimension and properties of single-slot MCA are shown in Table 1. The goal of this treatment treated liver by MW heating and without damaged to the surrounding tissue.

In this study, the liver cancer domain based on the porous media model. The porous liver cancer consists of 2 domains, the porous tumor, and the porous healthy tissue. The center of the tumor sets on the center slot and tumor radius of 10 mm. All domains are considered as an axisymmetric model, which the geometry of porous liver cancer, as shown in Fig. 1(a). The porous tissue domains (tumor and healthy tissue domain) are based on LTE in the porous media theory. The geometry of the model based on Bioheat was adapted to the geometry of the porous liver. In this study, the liver cancer model with MW ablation by using single-slot MCA for all cases. The mathematical of the porous model is considered to couple with the electromagnetic wave propagation, heat transfer, and fluid (blood) flow based on LTE assumption. The dielectric and thermal properties of the model are selected from the literature [2,26,36,37], as shown in Table 2.

2.2. Equations of electromagnetic wave propagation analysis

The electromagnetic (EM) wave propagation was considered in all domains. The governing equations and boundary conditions of EM wave propagation were applied for all models.

2.2.1. Governing equation and assumptions of electromagnetic wave propagation analysis

The electromagnetic wave propagation is considered in all domains. To reduce the complexity of the problem, the following assumptions are made.

1. The electromagnetic wave propagation considered in the 2-D axisymmetric model on r-z coordinates.
2. The electromagnetic wave propagation in the MCA is characterized by transverse electromagnetic fields (TEM) [38].
3. The electromagnetic wave propagation is characterized by transverse magnetic fields (TM) [38].
4. The model assumes that the dielectric properties of the liver are uniform.

The propagation of the electromagnetic wave in the antenna is by a transverse electromagnetic field (TEM) [2] that given as:

$$\text{Electric field } (\vec{E}) \vec{E} = E_r \frac{C}{r} E^{j(\omega t - kz)} \tag{1}$$

$$\text{Magnetic field } (\vec{H}) \vec{H} = E_\phi \frac{C}{rZ} E^{j(\omega t - kz)} \tag{2}$$

where  $\vec{E}$  is the electric field (V/m),  $r, \phi$ , and  $z$  are cylindrical coordinates centered on the axis of the coaxial cable.  $C = \sqrt{\frac{ZP_{in}}{\pi \cdot \ln(R_{outer}/R_{inner})}}$  is the arbitrary constant,  $Z$  is the wave impedance ( $\Omega$ ),  $P_{in}$  is the MW power input (W),  $R_{outer}$  is the dielectric outer radius (m),  $R_{inner}$  is the dielectric inner radius (m),  $f$  is the frequency (Hz),  $\omega = 2\pi f$  is the angular frequency (rad/s),  $k$  is the wave propagation constant ( $m^{-1}$ ), which relates to the wavelength ( $\lambda$ ) in medium:  $k = \frac{2\pi}{\lambda}$ .

Furthermore, the propagation of the electromagnetic wave in the biological tissue is by a transverse magnetic field (TM) as described by the following equation:

$$\nabla \times \left( \left( \frac{1}{\epsilon_r} - \frac{j\sigma_{el}}{\omega\epsilon_0} \right)^{-1} \nabla \times \vec{H}_\theta \right) - \mu_r k_0^2 \vec{H}_\theta = 0 \tag{3}$$

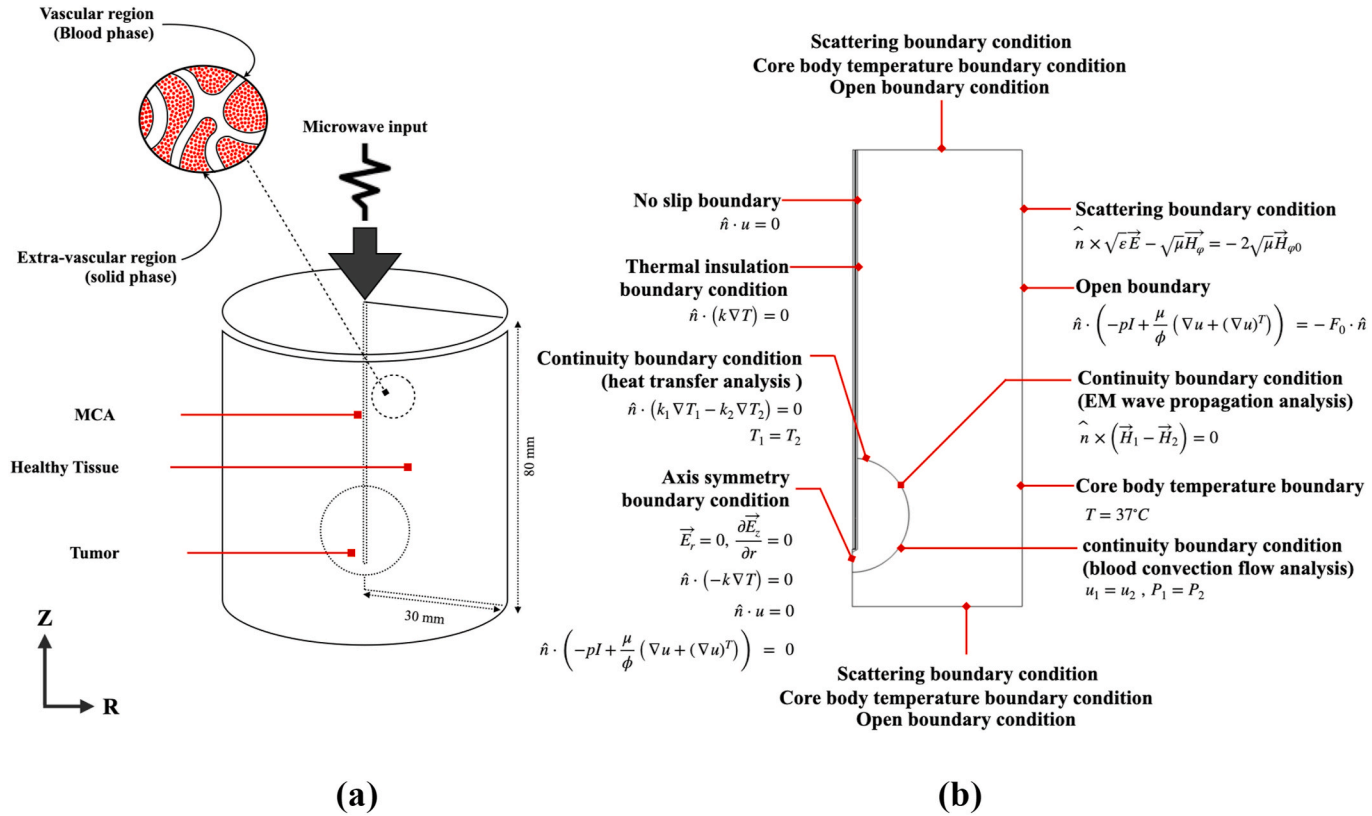


Fig. 1. The physical domain and boundary conditions of porous liver cancer model with MW ablation; (a) The physical domain, (b) The boundary conditions.

**Table 2**  
The dielectric and thermal properties of the tissue [26,37].

properties	Normal Tissue	Tumor	Blood
Relative permittivity, $\epsilon_r$	43	48.16	58.3
Electric conductivity, $\sigma_{el}$ (S/m)	1.69	2.096	2.54
Density, $\rho$ (kg/m <sup>3</sup> )	1030	1040	1058
Thermal conductivity, $k_{th}$ (W/m <sup>2</sup> ·°C)	0.497	0.57	0.45
Specific heat capacity $C_p$ (J/kg·°C)	3600	3960	3960

where  $\vec{H}_\theta$  is magnetic field intensity (A/m),  $\mu_r$  is relative permeability,  $\epsilon_r$  is relative permittivity,  $\epsilon_0 = 8.8542 \times 10^{-12}$  F/m is permittivity of free space,  $\sigma_{el}$  is electric conductivity (S/m),  $k_0$  is the free space wavenumber (m<sup>-1</sup>), and  $\omega = 2\pi f$  is the angular frequency (rad/s).

The interaction of an electromagnetic wave with biological tissue can be defined in terms of a specific absorption rate (SAR) distribution. When the electromagnetic wave is transmitted by an MCA, it passes through it and then propagates throughout the entire domain. The electromagnetic wave is absorbed and converted to the external heat source term. In this study, SAR represents the MW power absorption deposited per unit mass in tissue (W/kg) [34]. The SAR is given by:

$$SAR = \frac{\sigma_{el}}{2\rho} |\vec{E}|^2 \tag{4}$$

where  $\sigma_{el}$  is the electrical conductivity (S/m),  $\rho$  is the tissue density (kg/m<sup>3</sup>), and  $\vec{E}$  is the electric field intensity (V/m).

**2.2.2. Boundary conditions of electromagnetic wave propagation analysis**

The boundary conditions of EM wave propagation were adapted for all cases. The EM boundary conditions of the porous liver show in Fig. 1(b), and the following conditions are made:

5. The outside of the computation domain is considered as a scattering boundary condition to eliminate the reflections:

$$\hat{n} \times \sqrt{\epsilon} \vec{E} - \sqrt{\mu_r} \vec{H}_\theta = 2\sqrt{\mu_r} \vec{H}_{\theta 0} \tag{5}$$

6. The interfaces between different mediums are considered as a continuity boundary condition:

$$\hat{n} \times (\vec{H}_1 - \vec{H}_2) = 0 \tag{6}$$

7. The boundary conditions of the inner and outer conductor of MCA as the perfect electric conductor (PEC) boundary conditions:

$$\hat{n} \times \vec{E} = 0 \tag{7}$$

8. The port boundary condition is applied at the inlet of MCA with the MW power level set to 10 W.
9. The electrical symmetry boundary condition is applied at  $r = 0$ :

$$\vec{E}_r = 0 \tag{8a}$$

$$\frac{\partial \vec{E}_z}{\partial r} = 0 \tag{8b}$$

**2.3. Equations of heat transfer and blood flow analysis**

In this study, the liver cancer model during MW ablation treatment was compared and applied by three heating models: the bioheat model, the porous model with constant velocity, and the Darcy-Brinkman porous model.

**2.3.1. Governing equation and assumptions of heat transfer and blood flow analysis**

The heat transfer and blood flow are considered in the tissue domains only, i.e., healthy tissue and tumor domain. For reduce the complexity of the problem, the assumptions of the Darcy-Brinkman porous model have been offered into the analysis:

10. Heat transfer, as well as heat convection, are considered in the 2-D axisymmetric model on r-z coordinates.
11. The liver tissue domains (healthy tissue and tumor) of the porous liver model are considered the homogeneous porous media materials, thermally isotropic, and saturated with blood.
12. The LTE heat transfer between solid and blood phases is considered.

13. The blood perfusion rate term is assumed to be constant for all cases.
14. The blood in the porous liver is incompressible and Newtonian.
15. The Boussinesq approximation is applied to the buoyancy term of the flow analysis.
16. The chemical reactions and phase changes are ignored.
17. The porosities and thermal properties of the porous liver are assumed to be constant and uniformed.
18. The analysis of heat transfer and flow in the MCA are ignored.

The heat transfer analysis of the porous liver model was considered the transient problem, and couples with electromagnetic wave propagation. The heat transfer in the liver tissue is obtained by solving the energy equation, which based on the LTE approach in porous media theory. The equations are given as follows:

$$(\rho C_p)_{eff} \frac{\partial T}{\partial t} + \rho_b C_{p,b} u \cdot \nabla T = k_{th,eff} \nabla^2 T + \rho_b C_{p,b} \omega_b (T_b - T) + Q_{met} + Q_{ext} \tag{9a}$$

$$(\rho C_p)_{eff} = (1 - \varphi)(\rho C_p)_s + \varphi(\rho C_p)_b \tag{9b}$$

$$k_{th,eff} = (1 - \varphi)k_{th,s} + \varphi k_{th,b} \tag{9c}$$

where, the subscription *eff*, *s*, *th* and *b* represent the effective value, solid phase, thermal and blood phase, respectively.  $\varphi$  is the porosity (volume fraction of the vascular space),  $\rho$  is the tissue density (healthy liver tissue or tumor) (kg/m<sup>3</sup>),  $C_p$  is the specific heat capacity (J/kg·°C),  $T$  is the temperature of tissue (°C),  $k_{th}$  is the thermal conductivity (W/m·°C),  $\rho_b$  is the blood density (kg/m<sup>3</sup>),  $\omega_b$  is the blood perfusion rate (1/s),  $Q_{met}$  is the metabolism heat source ( $Q_{met} = 33,800$  W/m<sup>3</sup>) [39] and  $Q_{ext}$  is the external heat source term (W/m<sup>3</sup>). The external heat source term is converted from SAR distribution, which is defined as:

$$Q_{ext} = \frac{\sigma_{el} |\vec{E}|^2}{2} = \rho \cdot SAR \tag{10}$$

where, the parameters are corresponding with equation (4). It well-known, the blood perfusion rate of the large tumor slower than that in the healthy tissue. For the healthy tissue, the blood perfusion rate is  $6.4 \times 10^{-3}$  1/s, while the blood perfusion rate of tumor is  $2.12 \times 10^{-3}$  1/s [36,40]. The blood perfusion rate was applied to a constant value in all cases.

The flow analysis was applied only, i.e., the Darcy-Brinkman porous model. The Brinkman equation extended Darcy equation was first developed by Brinkman [41], and used for investigating the blood flow in the Darcy-Brinkman porous model. The governing equations describing the flow phenomenon in the Darcy-Brinkman porous model are given as follows [34]:

Continuity equation

$$\rho \nabla \cdot (u) = 0 \tag{11}$$

Momentum equation

$$\rho_b \frac{\partial u}{\partial t} = \left( -\rho I + \frac{\mu}{\varphi} (\nabla u + (\nabla u)^T) \right) - \frac{\mu u}{\kappa} + F \tag{12}$$

where  $u$  is the blood velocity (m/s),  $p$  is the pressure in porous liver (Pa),  $\mu = 0.003$  Pa/s is the viscosity of blood [42],  $F = g\beta(T - T_i)$  is the body force that applied the buoyancy term,  $\beta = 1 \times 10^{-4}$  1/K is the coefficient of thermal expansion,  $T_i$  is the reference temperature (°C), which is considered as the initial temperature of model, and  $\kappa$  is the permeability (m<sup>2</sup>), which can be expressed by the following [43,44]:

$$\kappa = \frac{\varphi^3 d_p^2}{175(1 - \varphi)^2} \tag{13}$$

where  $d_p = 1 \times 10^{-4}$  m<sup>2</sup> is the diameter of tissue cells. The inertial effect of blood flow was relatively low, which was neglected [34].

In order to implement the porous model with constant velocity in the porous liver model, the governing equation is equation (9) but ignore equation 11 and 12 [26]. Also, the heat transfer for the bioheat model was considered the transient problem, and couples with electromagnetic wave propagation. The heat transfer in the liver tissue is obtained by solving only the bioheat equation [45,46]. The equation is given by:

$$\rho_s C_{p,s} \frac{\partial T}{\partial t} = k_{th,s} \nabla^2 T + \rho_b C_{p,b} \omega_b (T_b - T) + Q_{met} + Q_{ext} \tag{14}$$

### 2.3.2. Boundary conditions of heat transfer and flow analysis

The boundary conditions of heat transfer and flow were applied for the porous liver models and the only boundary conditions of heat transfer was applied the bioheat liver model. The boundary conditions of porous liver model were shown in Fig. 1(b), and to following conditions are made:

19. The top, right, and bottom sides of the liver domain is assumed to be constant the core body temperature for the bioheat and

porous models, as shown in Equation (15a). Furthermore, the top, right, and bottom sides of the porous models are assumed to be open boundary conditions, as shown in Equation (15b).

$$T = 37^\circ\text{C} \quad (15a)$$

$$\hat{n} \cdot \left( -pI + \frac{\mu}{\varphi} (\nabla u + (\nabla u)^\tau) \right) = -F_0 \cdot \hat{n} \quad (15b)$$

20. The interfaces between the healthy tissue and the tumor are considered as the thermal and flow continuity boundary conditions for the porous models, as shown in Equations (16a) - (16d). The interfaces between the healthy tissue and the tumor are considered as only the thermal continuity boundary conditions for the bioheat model, as shown in Equations (16a) - (16b).

$$\hat{n} \cdot (k_1 \nabla T_1 - k_2 \nabla T_2) = 0 \quad (16a)$$

$$T_1 = T_2 \quad (16b)$$

$$u_1 = u_2 \quad (16c)$$

$$P_1 = P_2 \quad (16d)$$

21. The interfaces of healthy tissue and tumors with MCA are considered thermally insulated for all models and no-slip boundary conditions for the only porous models.

$$\hat{n} \cdot (k \nabla T) = 0 \quad (17a)$$

$$\hat{n} \cdot u = 0 \quad (17b)$$

$$\hat{n} \cdot \left( -pI + \frac{\mu}{\varphi} (\nabla u + (\nabla u)^\tau) \right) = 0 \quad (17c)$$

22. The thermal symmetry boundary conditions are applied  $r = 0$  for all models and including the symmetry of flow boundary conditions for only the porous models.

$$\hat{n} \cdot (k \nabla T) = 0 \quad (18a)$$

$$\hat{n} \cdot u = 0 \quad (18b)$$

$$\hat{n} \cdot \left( -pI + \frac{\mu}{\varphi} (\nabla u + (\nabla u)^\tau) \right) = 0 \quad (18c)$$

#### 2.4. Initial condition

The initial electromagnetic fields of the models are set to 0 V/m, the initial temperature of the models is set to the core temperature, which of 37 °C, while the initial velocity is set of 0 m/s.

### 3. Calculation procedure

This study developed the numerical of liver cancer model with MW ablation based on the LTE porous media model. The numerical models are solved by the FEM to analyze a 2D axisymmetric transient problem. The EM wave propagation analysis was applied in all domains. The heat transfer and blood flow were applied only tissue domains (healthy tissue and tumor domain). The performing comparative of predicted thermal models during MW ablation: the bioheat model, the porous model with constant velocity, and the Darcy-Brinkman porous model were investigated on the heat transfer in the identical condition. The numerical models were discretized using triangular elements with Lagrange quadratic shape functions, and the elements were adaptive in sensitive areas. The initial time-steps and the maximum time-steps to solve the transient problem were  $1 \times 10^{-4}$  s and 0.1 s, respectively. The convergence test for the liver cancer model is showing the relation with the temperature at the sensitive point. The density of elements, approximately 41,720 elements, was mesh independent. Increasing the number of elements past this point did not lead to significantly different computational results. All simulations are computed with 2D symmetry FEM analysis by using COMSOL™ Multiphysics.

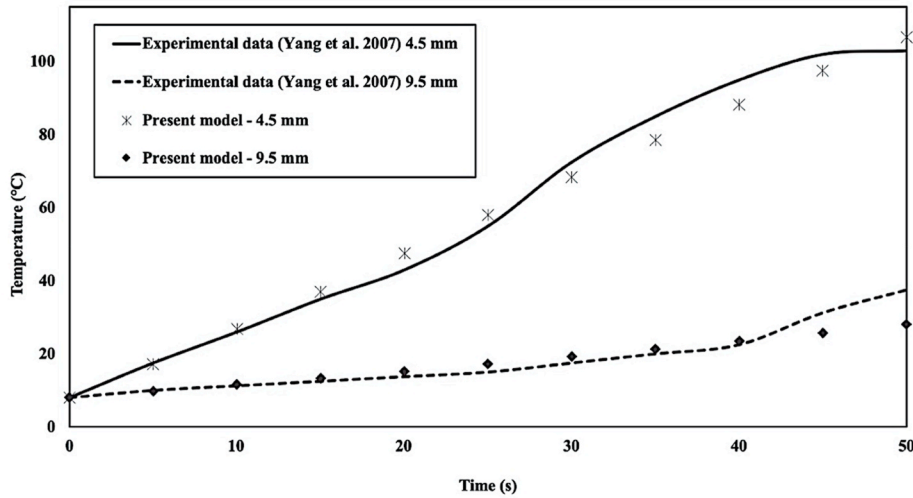


Fig. 2. The validation results of the calculated tissue temperature to the tissue temperature obtained by Yang et al. [29].

Table 3

Comparisons of RMSE of the liver tissue temperature between the presented model and Yang et al. [2,29].

Position (mm)	Comparisons of RMSE with experiment from Yang et al., (°C)	
	Presented study (Brinkman)	Yang et al. (simulation model)
4.5	3.95	11.03 [2]
9.5	3.50	5.57 [2]

## 4. Results and discussion

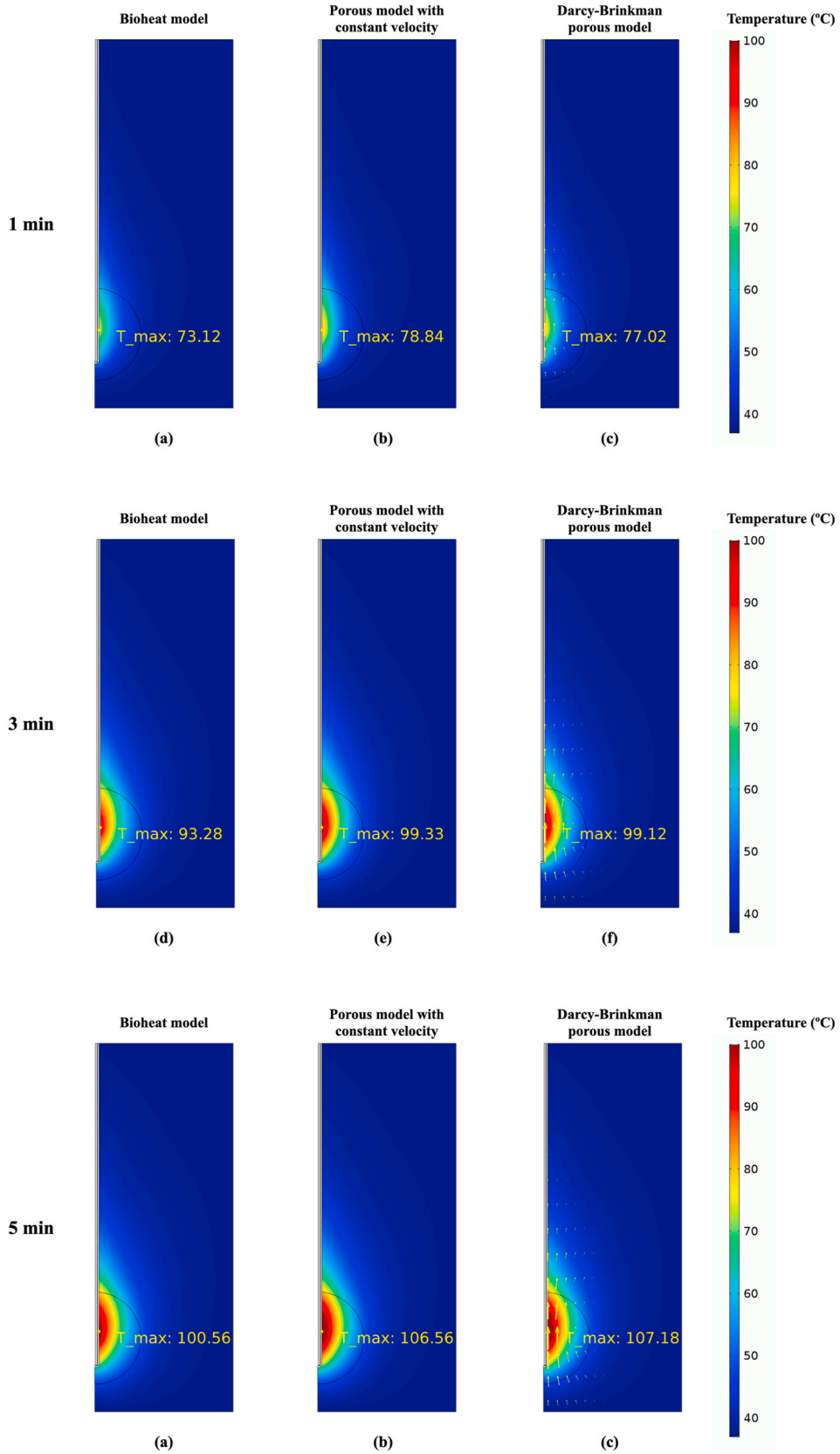
### 4.1. Verification of model

In order to verify the accuracy of the present numerical study, the present numerical model was validated against the experimental results obtained by Yang et al. [29] for the MW ablation of the bovine liver under the same testing conditions. In the validation model, the MW power input was 75 W with a frequency of 2.45 GHz, and the initial temperature of the liver domain was set to 8 °C. The MCA was inserted 20 mm deep into the liver tissue, and the duration for a heating time was 180 s. The simulation results against the experimental results received by literature [29] are shown in Fig. 2, which shows the temperature of two points 4.5 and 9.5 mm away from the MCA, in dependence on the heating time. The error between the presented model and Yang et al.’s experiment results shows in Table 3. The simulation results are clearly in good agreement with the experimental results. This gives confidence in the accuracy of the presented numerical models.

### 4.2. The comparative of the performance of thermal models

In this section, the MW ablation technique is used to treat in the liver cancer with MW power of 10 W, a frequency of 2.45 GHz, and a heating time period of 5 min for all cases. The mathematical models considered couple with the EM wave propagation, heat transfer, and flow analysis. The three liver cancer models were applied the bioheat model, the porous model with constant velocity, and the Darcy-Brinkman porous model. The EM wave propagation analysis based on the same governing equations and conditions. Thus, the EM wave propagation with the bioheat model, the porous model with constant velocity, and the Darcy-Brinkman porous model was identical. Fig. 3 shows the 2D-plot temperature and blood velocity vector of the bioheat model, the porous model with constant velocity, and the Darcy-Brinkman porous model for a heating time of 1, 3, and 5 min. The high temperature zone or the hot spot area of the liver cancer model has appeared around the slot area and decrease with distance from the slot. The hot spot area in the liver cancer model was similar to the water of droplet. The temperature was distributed in the direction of antenna insertion (z-axis) more than the radius side (r-axis). Besides, the temperature profiles of the bioheat model, the porous model with constant velocity, and the Darcy-Brinkman porous model were similarly distributed.

However, Fig. 3 shows the maximum temperature of the three heating models, and they were different. The maximum temperature of the bioheat model was 73.12 °C, 93.28 °C, and 100.56 °C for the heating time of 1 min, 3 min, and 5 min, respectively (shown in Fig. 3(a), (d), and 9(g)). The maximum temperature of the porous model with constant velocity was 78.84 °C, 99.33 °C, and 106.56 °C (shown in Fig. 3(b), (e), and 3(h)). The maximum temperature of the Darcy-Brinkman porous model was 77.02 °C, 99.12 °C, and



(caption on next page)

**Fig. 3.** The temperature distribution and velocity vector of the difference liver cancer models with MW ablation for a heating time of 1, 3, and 5 min, the MW power of 10 W, and frequency of 2.45 GHz.

107.18 °C (shown in Fig. 3(c), (f), and 3(i)). In all the figures henceforth, the arrows represent the direction and the magnitude of blood velocity in the liver domain. The maximum temperature of the three models increased with the heating time. The maximum temperature of the porous model with constant velocity shows the highest temperature, followed by the Darcy-Brinkman porous model and the bioheat model, respectively. The maximum temperature of the porous model with constant velocity and the Darcy-Brinkman porous model was similar trend when the heating time increased. This because in the early state, the heat transfer of the Darcy-Brinkman porous model plays the role of conduction. After that, the heat convection of the Darcy-Brinkman porous model increased and forcefully when the heating time increased. Furthermore, the heat transfer of the Darcy-Brinkman porous model is strongly convection with the heating time increased. The blood convection flow is driven by the effect of the buoyancy term, which is increased by the gradient temperature in the model. These comparative results show the porous models' maximum temperatures (with the constant velocity and the Darcy-Brinkman) similarly when the heating time increased.

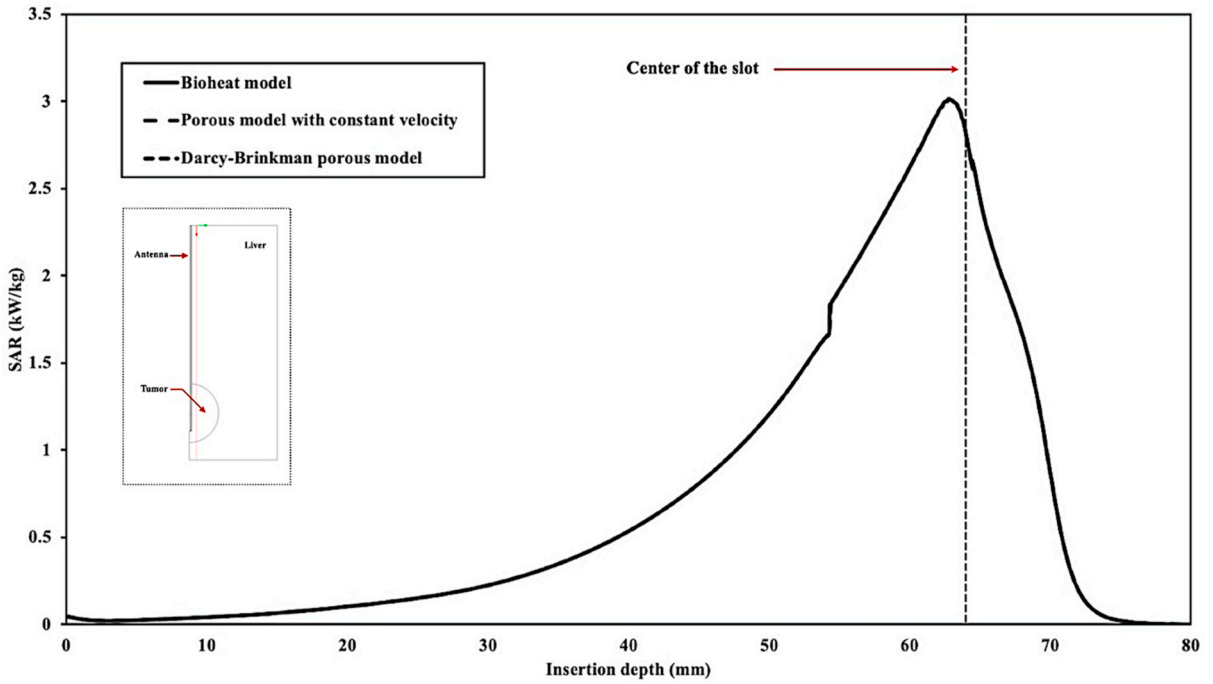
In this study, the MW propagation in the liver tissue (i.e., healthy tissue and tumor) is considered axisymmetric propagation and the characterization with TM mode. When the MW penetration in the tissue, the MW is contributed to the heat generation in liver tissue by using the dipole rotation mechanism. The goal of this treatment is to destroy the target tissue by without damaged in the surrounding healthy tissue. The electromagnetic wave propagation is the first mechanism for this treatment. Therefore, electromagnetic wave propagation has to investigate. Fig. 4(a) shows the SAR distribution of the liver cancer models at the insertion depth line. The SAR distribution is strongly distributed near a slot of the antenna and decreased with distance from a slot. In this simulation results, the SAR of all models is similarly profiles. That because electric field intensity and the dielectric properties of all models are nearly the same. The temperature distribution in Fig. 4(b) is a similar trend with the SAR distribution, but the temperature between each models is different, especially in the hot spot zone.

The insertion line in the liver cancer model was the line to parallel with MCA and away from MCA of 2.5 mm ( $r = 2.5$  mm), as shown in Fig. 4. Fig. 4(b) shows the temperature distribution of the liver cancer models along with the insertion depth line for a heating time of 1, 3, and 5 min. The maximum temperature of all models appeared around the slot area and decreased with distance away from the slot. The temperature distribution increases with heating time. In the hot spot zone, the temperature of the liver cancer model with the different models is clearly the difference. In the early stage of heating, the temperature distribution between models is slightly different. When treatment time increases, the temperature distribution between the bioheat model and the porous models were clearly different. Furthermore, the temperature distribution of the porous model with constant velocity and the Darcy-Brinkman porous model was seemed to be the trend. This because the effect of heat convection was increasing when the gradient temperature was increasing. Moreover, the temperature difference between the porous model with constant velocity and the Darcy-Brinkman porous model was decreasing with heating time, corresponding with the result from Fig. 3.

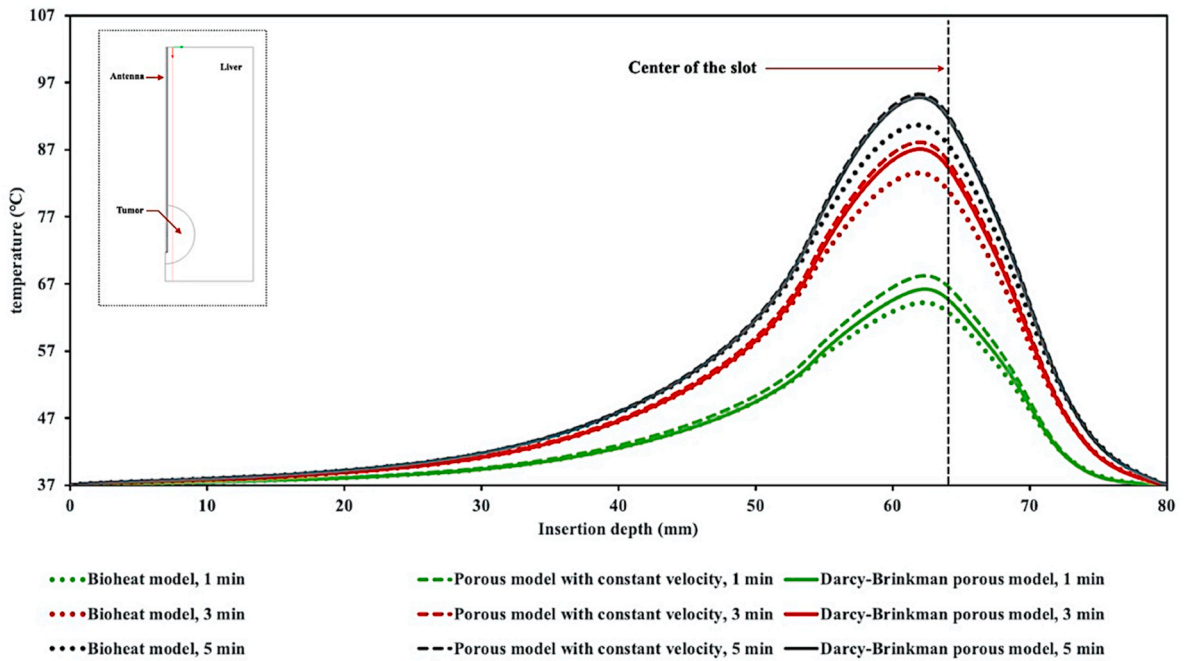
The position of the temperature monitoring points at the center of the slot line, which P2 position is a point at the boundary of the tumor and along with the center of the slot line, as shown in Fig. 5. Left hand side of P2, these points are monitoring the temperature in the tumor domain. Right hand side, the points on the right side of the P2 monitoring the temperature in the healthy liver domain. Fig. 5 shows the temperature distribution of the liver cancer model at the monitoring points with a heating time of 1, 3, 5 min. The temperature of the left hand side was higher than the right hand side. The temperature distribution of the porous model with constant velocity was most quickly increasing, followed by the Darcy-Brinkman porous model and bioheat model, respectively. In the hot spot zone (left side), the temperature distribution of the liver cancer with different thermal models implemented have clearly seen the difference. In case of porous model, the stronger heat convection clearly observed in the high temperature area, because in this area, the blood convection is strongly dependent with gradient temperature. However, the distance away from the slot could not observe the effect of the different thermal models on the temperature distribution. Furthermore, the temperature distribution of the porous model with constant velocity and the Darcy-Brinkman porous model is a similar trend, when the heating time increases, corresponding with Figs. 3 and 4.

Fig. 6(a) shows the percentage of the damaged area of the models. The damaged area of the liver cancer model with the MW ablation was calculated by integrating the area, in which the temperature of the area increases over 52 °C. This integrating area was divided by the total area. This section represented the area as the specific tumor area, the specific healthy liver area, and the total area. The total area was a combination of the area of the tumor and healthy liver. The damaged area increases with the heating time. The most percentage of damage has occurred in the tumor area, followed by the total area (tumor area, including healthy liver) and the healthy liver, respectively. The effect of the thermal models implemented on the percentage of the damaged area could be seen in the only tumor, as the hot spot area has appeared in the tumor area. The damaged area of the thermal models was corresponding with the temperature distribution. For the heating time of 5 min, the tumor damage of 82.75%, 83.75%, and 83.30% for the bioheat model, the porous model with constant velocity, the Darcy-Brinkman porous model, respectively. Simultaneously, the healthy liver damage of 2.54%, 2.59%, and 2.59% for the bioheat model, the porous model with constant velocity, and the Darcy-Brinkman porous model, respectively. Although this treatment was damaged on the healthy liver, nevertheless, it is only a small amount of destruction (less than 3% also all models).

The Root Mean Square Error (RMSE) of the temperature difference between the bioheat model, the porous model with constant velocity, and the Darcy-Brinkman porous model shows in Fig. 6(b). The RMSE of the porous models (the porous model with constant velocity and the Darcy-Brinkman porous model) decreases with the heating time. On the other hand, the RMSE of the porous models and the bioheat model increases with the heating time. The RMSE of the porous model with constant velocity and the bioheat model



(a)



(b)

Fig. 4. The SAR and temperature distribution of the difference liver cancer models at the insertion depth line with MW power of 10 W, and frequency of 2.45 GHz.; (a) The SAR distribution, (b) The temperature distribution.

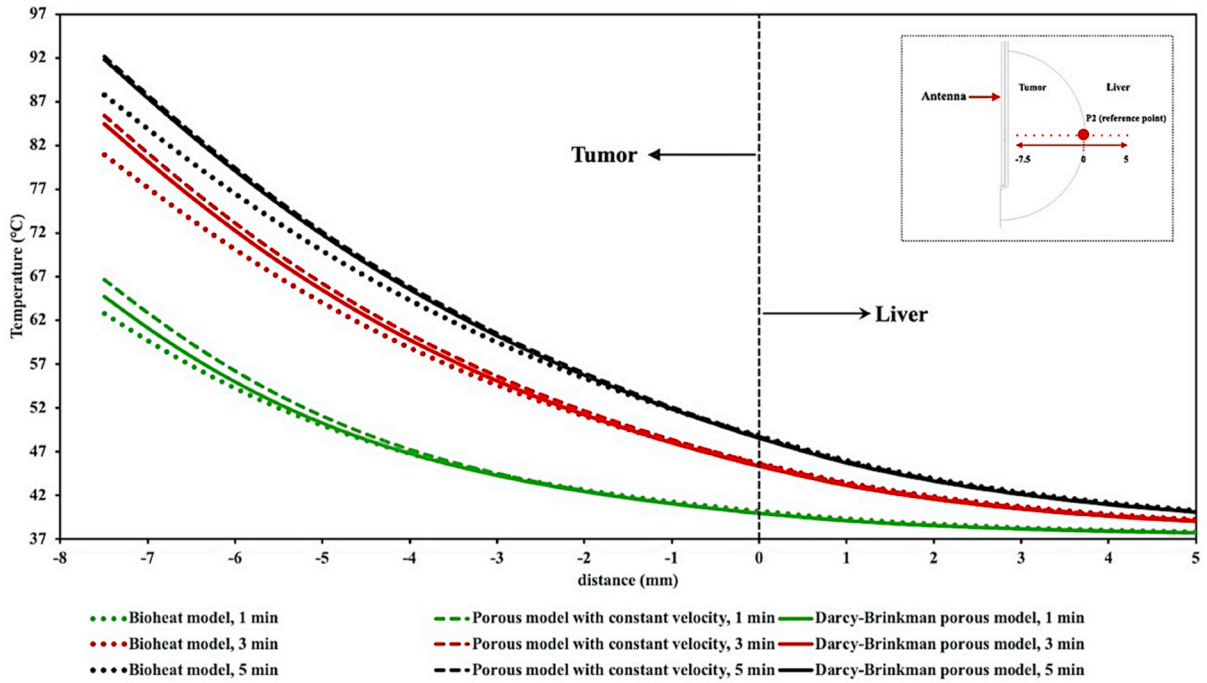


Fig. 5. The temperature distribution of the difference liver cancer models along at the monitoring points for a heating time of 1, 3, 5 min with the MW power of 10 W, and frequency of 2.45 GHz.

more than the Darcy-Brinkman porous model and the bioheat model. In the initial heating time, the heat transfer of Darcy-Brinkman porous model plays in the role of conduction mode. However, when the heating time increased, the heat transfer of the Darcy-Brinkman porous model plays in the role of convection combined with conduction modes. These results were shown on the temperature profiles difference between the Darcy-Brinkman porous model, the Bioheat, and the porous model with velocity constant.

In the early stage of the heating time, the effect of the thermal models implemented on the temperature distribution was not different. Because of the heat transfer of the early state was influenced by the heat conduction. After that, the temperature distribution of the thermal models implemented could be differently increased. In particular, the hot spot zones could clearly see the temperature differences. When increasing the heating time, the heat convection of the Darcy-Brinkman porous model has become stronger. It was seen to be the temperature of the Darcy-Brinkman porous model has similarly distributed the temperature of the porous model with constant velocity. Thus, the heat transfer of this state was driven by the heat convection more than the heat conduction. Furthermore, in the initial stage of heating time, the bioheat model could be implemented for the prediction temperature in the liver cancer model at an area far away from the hot spot. However, in the area of high temperature have to use the Darcy-Brinkman porous model for the prediction temperature in liver cancer model.

5. Conclusion

This work presents the numerical study of the heat transfer as well as the heat convection coupled with the EM wave propagation in the porous liver cancer model. The performing comparative of the predicted thermal models during the MW ablation process using a slot antenna with MW power of 10 W and frequency of 2.45 GHz was systematically investigated. The bioheat model, the porous model with constant velocity, and the Darcy-Brinkman porous model were implemented in the liver cancer model. The simulation of the porous model was in good agreement with the experimental results obtained by Yang et al. [29], as shown in Fig. 2. Key findings that occurred from this study:

- 23. The heating models have affected on temperature prediction in liver cancer model with MW ablation. Especially, in the area of the high temperature. In this area, The Darcy-Brinkman porous model has a flexible used than the porous model with constant velocity and the bioheat model. However, in the area far away from the hot spot, the three heating models have not different.
- 24. The effect of the different heating models on the heat transfer had clearly appeared in the hot spot area and similarly distributed in the area far away from the hot spot.
- 25. In the early stage of heating time, the heat transfer of the Darcy-Brinkman porous model and the bioheat model were roughly similar. When the heating time increased, the heat transfer of the Darcy-Brinkman porous model and the porous model with constant velocity were seemed to be the trend.

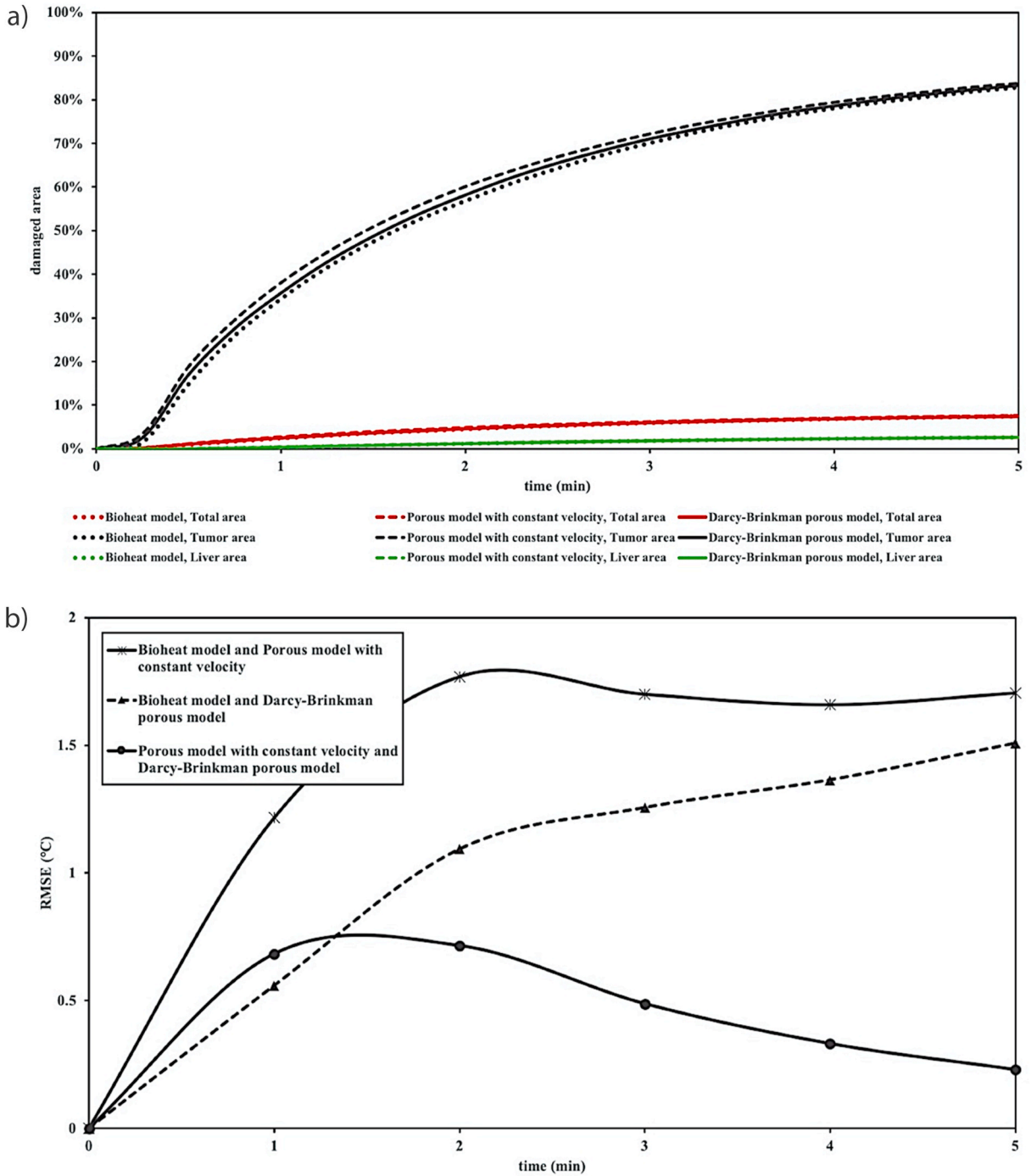


Fig. 6. (a) The percentage of the damaged area in the difference liver cancer models with the MW power of 10 W and the MW frequency of 2.45 GHz. Fig. 6(b) The RMSE of the comparative temperatures with the different thermal models implemented in the liver cancer model with MW ablation for the MW power of 10 W and the MW frequency of 2.45 GHz.

26. In the early stage of heating time, the effect of the thermal models implemented on the temperature distribution was not different. After that, the temperature distribution of the thermal models implemented could be differently increased. Because of the heat convection is strongly dependent with gradient temperature.

The four key findings could be concluded the effect of the thermal models on the heat transfer was necessary for consideration in the liver cancer treatment, especially in the high temperature area. The Darcy-Brinkman porous model was effective in various

situations, such as the role of conduction or the role of convection, or combination heat transfer. Therefore, the Darcy-Brinkman porous model was suggested for the heat transfer prediction in liver cancer model with the MW ablation technique, especially in the high temperature areas and the highest MW power.

The difference point between the porous model and the bioheat can be expressed in the difference in the equations. The equation of the bioheat model based on heat diffusion. This equation added blood perfusion term in the heat conduction equation. The heat transfer mechanism of the bioheat model plays in the role of conduction. On the other hand, the equation of the porous media based on heat convection. In the early state of heating, heat transfer plays in the role of conduction. Therefore, the temperature distribution is slightly different between porous models and bioheat model. After that, the heat transfer of the porous models plays in the role of convection. Nevertheless, the heat transfer of the bioheat still plays in the role of conduction. It is not a suggestion for the medium and extended state of heating time, in which heat transfer of the bioheat and porous models occurs differently.

In the next step of this research, we will develop the numerical modeling for approaching realistic liver tissue will be performed with the deformation analysis in the porous liver. The study will also consider the local non-thermal equilibrium (LNTE) heat transfer model in analyzing biological tissues subjected to MW energy.

#### Author statement

Wutipong Preechaphonkul: Conceptualization, Methodology, Writing, Software and Validation. Phadungsak Rattanadecho: corresponding author, Conceptualization, and supervision.

#### Declaration of competing interest

The authors declare that they have no known competing financial interests or personal relationships that could have appeared to influence the work reported in this paper.

#### Acknowledgments

The authors gratefully acknowledge the Thailand Science Research and Innovation (under the Royal Golden Jubilee Ph.D. Program (RGJ) grant number PHD/0055/2558) and the Program Management Unit for Human Resources & Institutional Development, Research and Innovation, NXPO (grant number B05F630092) provided financial support for this study.

#### References

- [1] R.C. Martin, C.R. Scoggins, K.M. McMasters, Safety and efficacy of microwave ablation of hepatic tumors: a prospective review of a 5-year experience, *Ann. Surg. Oncol.* 17 (1) (2010) 171–178.
- [2] P. Keangin, P. Rattanadecho, T. Wessapan, An analysis of heat transfer in liver tissue during microwave ablation using single and double slot antenna, *Int. Commun. Heat Mass Tran.* 38 (6) (2011) 757–766.
- [3] C. Correa-Gallego, Y. Fong, M. Gonen, M.I. D'Angelica, P.J. Allen, R.P. DeMatteo, T.P. Kingham, A retrospective comparison of microwave ablation vs. radiofrequency ablation for colorectal cancer hepatic metastases, *Ann. Surg. Oncol.* 21 (13) (2014) 4278–4283.
- [4] G.J. Poston, D. Tait, S. O'Connell, A. Bennett, S. Berendse, Diagnosis and management of colorectal cancer: summary of NICE guidance, *BMJ* 343 (2011) d6751.
- [5] B.W. Dong, P. Liang, X.L. Yu, X.Q. Zeng, P.J. Wang, L. Su, S.O.N.G. Li, Sonographically guided microwave coagulation treatment of liver cancer: an experimental and clinical study, *AJR. American journal of roentgenology* 171 (2) (1998) 449–454.
- [6] S.N. Goldberg, G.S. Gazelle, P.R. Mueller, Thermal ablation therapy for focal malignancy: a unified approach to underlying principles, techniques, and diagnostic imaging guidance, *Am. J. Roentgenol.* 174 (2) (2000) 323–331.
- [7] W.M. Whelan, S.R.H. Davidson, L.C.L. Chin, I.A. Vitkin, A novel strategy for monitoring laser thermal therapy based on changes in optothermal properties of heated tissues, *Int. J. Thermophys.* 26 (1) (2005) 233–241.
- [8] P. Prakash, G. Deng, M.C. Converse, J.G. Webster, D.M. Mahvi, M.C. Ferris, Design optimization of a robust sleeve antenna for hepatic microwave ablation, *Phys. Med. Biol.* 53 (4) (2008) 1057.
- [9] P. Prakash, V.A. Salgaonkar, E. Clif Burdette, C.J. Diederich, Multiple applicator hepatic ablation with interstitial ultrasound devices: theoretical and experimental investigation, *Med. Phys.* 39 (12) (2012) 7338–7349.
- [10] T. Wu, P. Li, Q. Shao, J. Hong, L. Yang, S. Wu, A simulation-experiment method to characterize the heat transfer in ex-vivo porcine hepatic tissue with a realistic microwave ablation system, *Numer. Heat Tran., Part A: Applications* 64 (9) (2013) 729–743.
- [11] F.Y. Liu, X.L. Yu, P. Liang, Y. Wang, P. Zhou, J. Yu, Comparison of percutaneous 915 MHz microwave ablation and 2450 MHz microwave ablation in large hepatocellular carcinoma, *Int. J. Hyperther.* 26 (5) (2010) 448–455.
- [12] J. Xu, Z.Z. Jia, Z.J. Song, X.D. Yang, K. Chen, P. Liang, Three-dimensional ultrasound image-guided robotic system for accurate microwave coagulation of malignant liver tumours, *Int. J. Med. Robot. Comput. Assist. Surg.* 6 (3) (2010) 256–268.
- [13] H. Ren, P. Liang, X. Yu, Y. Wang, T. Lu, X. Li, Treatment of liver tumours adjacent to hepatic hilum with percutaneous microwave ablation combined with ethanol injection: a pilot study, *Int. J. Hyperther.* 27 (3) (2011) 249–254.
- [14] G. Carrafiello, D. Laganà, M. Mangini, F. Fontana, G. Dionigi, L. Boni, C. Fugazzola, Microwave tumors ablation: principles, clinical applications and review of preliminary experiences, *Int. J. Surg.* 6 (2008) S65–S69.
- [15] C.L. Brace, Radiofrequency and microwave ablation of the liver, lung, kidney, and bone: what are the differences? *Curr. Probl. Diagn. Radiol.* 38 (3) (2009) 135–143.
- [16] X. Li, L. Zhang, W. Fan, M. Zhao, L. Wang, T. Tang, Y. Liu, Comparison of microwave ablation and multipolar radiofrequency ablation, both using a pair of internally cooled interstitial applicators: results in ex vivo porcine livers, *Int. J. Hyperther.* 27 (3) (2011) 240–248.
- [17] A.D. Strickland, P.J. Clegg, N.J. Cronin, B. Swift, M. Festing, K.P. West, D.M. Lloyd, Experimental study of large-volume microwave ablation in the liver, *Br. J. Surg.* 89 (8) (2002) 1003–1007.
- [18] A.U. Hines-Peralta, N. Pirani, P. Clegg, N. Cronin, T.P. Ryan, Z. Liu, S.N. Goldberg, Microwave ablation: results with a 2.45-GHz applicator in ex vivo bovine and in vivo porcine liver, *Radiology* 239 (1) (2006) 94–102.
- [19] P. Saccomandi, E. Schena, C. Massaroni, Y. Fong, R.F. Grasso, F. Giurazza, R.L. Cazzato, Temperature monitoring during microwave ablation in ex vivo porcine livers, *Eur. J. Surg. Oncol.* 41 (12) (2015) 1699–1705.

- [20] V. Lopresto, R. Pinto, L. Farina, M. Cavagnaro, Microwave thermal ablation: effects of tissue properties variations on predictive models for treatment planning, *Med. Eng. Phys.* 46 (2017) 63–70.
- [21] C. Marcelin, J. Leiner, S. Nasri, F. Petitpierre, Y. Le Bras, M. Yacoub, F. Cornelis, In vivo percutaneous microwave ablation in kidneys: correlation with ex vivo data and ablation work, *Diagnostic and interventional imaging* 99 (1) (2018) 3–8.
- [22] H.H. Pennes, Analysis of tissue and arterial blood temperatures in the resting human forearm, *J. Appl. Physiol.* 1 (2) (1948) 93–122.
- [23] J. Okajima, S. Maruyama, H. Takeda, A. Komiya, Dimensionless solutions and general characteristics of bioheat transfer during thermal therapy, *J. Therm. Biol.* 34 (8) (2009) 377–384.
- [24] P. Phasukkit, S. Tungjitkusolmun, M. Sangworasil, Finite-element analysis and in vitro experiments of placement configurations using triple antennas in microwave hepatic ablation, *IEEE (Inst. Electr. Electron. Eng.) Trans. Biomed. Eng.* 56 (11) (2009) 2564–2572.
- [25] M. Liangruksa, R. Ganguly, I.K. Puri, Parametric investigation of heating due to magnetic fluid hyperthermia in a tumor with blood perfusion, *J. Magn. Magn. Mater.* 323 (6) (2011) 708–716.
- [26] P. Keangin, P. Rattanadecho, Analysis of heat transport on local thermal non-equilibrium in porous liver during microwave ablation, *Int. J. Heat Mass Tran.* 67 (2013) 46–60.
- [27] H.G. Klinger, Heat transfer in perfused biological tissue—I: general theory, *Bull. Math. Biol.* 36 (1974) 403–415.
- [28] W. Wulff, The energy conservation equation for living tissue, *IEEE Trans. Biomed. Eng.* (6) (1974) 494–495.
- [29] D. Yang, M.C. Converse, D.M. Mahvi, J.G. Webster, Expanding the bioheat equation to include tissue internal water evaporation during heating, *IEEE (Inst. Electr. Electron. Eng.) Trans. Biomed. Eng.* 54 (8) (2007) 1382–1388.
- [30] X. Wu, B. Liu, B. Xu, Theoretical evaluation of high frequency microwave ablation applied in cancer therapy, *Appl. Therm. Eng.* 107 (2016) 501–507.
- [31] S. Mahjoob, K. Vafai, Analytical characterization of heat transport through biological media incorporating hyperthermia treatment, *Int. J. Heat Mass Tran.* 52 (5–6) (2009) 1608–1618.
- [32] W. Roetzl, Y. Xuan, Transient response of the human limb to an external stimulant, *Int. J. Heat Mass Tran.* 41 (1) (1998) 229–239.
- [33] A. Nakayama, F. Kuwahara, A general bioheat transfer model based on the theory of porous media, *Int. J. Heat Mass Tran.* 51 (11–12) (2008) 3190–3199.
- [34] P. Rattanadecho, P. Keangin, Numerical study of heat transfer and blood flow in two-layered porous liver tissue during microwave ablation process using single and double slot antenna, *Int. J. Heat Mass Tran.* 58 (1–2) (2013) 457–470.
- [35] P. Keangin, K. Vafai, P. Rattanadecho, Electromagnetic field effects on biological materials, *Int. J. Heat Mass Tran.* 65 (2013) 389–399.
- [36] Y.L. Shao, B. Arjun, H.L. Leo, K.J. Chua, Nano-assisted radiofrequency ablation of clinically extracted irregularly-shaped liver tumors, *J. Therm. Biol.* 66 (2017) 101–113.
- [37] S. Koksungnoen, P. Rattanadecho, P. Wongchadaku, 3D numerical model of blood flow in the coronary artery bypass graft during no pulse and pulse situations: effects of an anastomotic angle and characteristics of fluid, *J. Mech. Sci. Technol.* 32 (9) (2018) 4545–4552.
- [38] J.M. Bertram, D. Yang, M.C. Converse, J.G. Webster, D.M. Mahvi, Antenna design for microwave hepatic ablation using an axisymmetric electromagnetic model, *Biomed. Eng. Online* 5 (1) (2006) 15.
- [39] Y. Rabin, A. Shitzer, Numerical Solution of the Multidimensional Freezing Problem during Cryosurgery, 1998.
- [40] R.K. Jain, K. Ward-Hartley, Tumor blood flow-characterization, modifications, and role in hyperthermia, *IEEE Trans. Son. Ultrason.* 31 (5) (1984) 504–525.
- [41] H.C. Brinkman, On the permeability of media consisting of closely packed porous particles, *Flow, Turbul. Combust.* 1 (1) (1949) 81.
- [42] M. Nabaee, M. Karimi, Numerical investigation of the effect of vessel size and distance on the cryosurgery of an adjacent tumor, *J. Therm. Biol.* 77 (2018) 45–54.
- [43] D.A. Nield, A. Bejan, *Convection in Porous Media*, vol. 3, Springer, New York, 2006.
- [44] K. Vafai, Convective flow and heat transfer in variable-porosity media, *J. Fluid Mech.* 147 (1984) 233–259.
- [45] T. Wessapan, P. Rattanadecho, Temperature induced in human organs due to near-field and far-field electromagnetic exposure effects, *Int. J. Heat Mass Tran.* 119 (2018) 65–76.
- [46] P. Wongchadaku, P. Rattanadecho, T. Wessapan, Implementation of a thermomechanical model to simulate laser heating in shrinkage tissue (effects of wavelength, laser irradiation intensity, and irradiation beam area), *Int. J. Therm. Sci.* 134 (2018) 321–336.